Accurate Gauge-Invariant Tensor-Network Simulations for Abelian Lattice Gauge Theory in $(2+1)$D: Ground-State and Real-Time Dynamics

Yantao Wu [1,*,†] and Wen-Yuan Liu [2,*,‡]
[1]Institute of Physics, Chinese Academy of Sciences, Beijing 100190, China
[2]Institute for Advanced Study in Physics, Zhejiang University, Hangzhou 310027, China

(Received 9 April 2025; revised 13 July 2025; accepted 2 September 2025; published 23 September 2025)

We propose a novel tensor-network method to achieve accurate and efficient simulations of Abelian lattice gauge theories (LGTs) in $(2+1)$D for both ground-state and real-time dynamics. The first key is to identify a gauge canonical form of gauge-invariant tensor-network states, which already simplifies existing algorithms for $(1+1)$D LGTs. The second key is to employ the gauge canonical form of a projected entangled-pair state (PEPS) combining with variational Monte Carlo, enabling efficient computations for $(2+1)$D LGTs. We demonstrate the versatile capability of this approach for accurate ground-state simulation of pure $\mathbb{Z}_2$, $\mathbb{Z}_3$, and $\mathbb{Z}_4$ gauge theory, odd-$\mathbb{Z}_2$ gauge theories, and $\mathbb{Z}_2$ gauge theory coupled to hard-core bosons, on square lattices up to 32×32. Furthermore, we demonstrate that it allows for accurate simulations of real-time dynamics up to long time, exemplified by the dynamics of elementary excitations of the deconfined $\mathbb{Z}_2$ gauge field at 10×10. This is also the first example of simulating the real-time dynamics of PEPS with variational Monte Carlo, whose impact may extend beyond gauge theory. Our Letter establishes gauge-invariant PEPS as a powerful approach for both ground-state and dynamical simulations, opening up a new avenue for nonperturbatively studying $(2+1)$D LGTs.

DOI: 10.1103/3m3j-ds18

Introduction—The study of lattice gauge theories (LGTs) constitutes a cornerstone in modern physics. They play foundational roles in quantum chromodynamics for studying quark confinement and hadron structure [1–3] and also provide critical insights into condensed matter physics, where low-energy effective theories of strongly correlated systems such as quantum spin liquids and topological orders have gauge structures [4,5]. The traditional Monte Carlo sampling of partition functions is a very successful computational paradigm for LGTs; however, it remains challenging for equilibrium properties plagued by sign problem [6] and real-time dynamics. These limitations have spurred intense efforts to develop computation in the Hamiltonian formulation, such as quantum simulations [7–11].

Tensor-network states (TNS) have emerged as a promising, sign-free classical simulation approach for LGTs [12–23]. In $(1+1)$D, TNS in the form of matrix product state (MPS) have been established as a reliable numerical methodology [14,24–28]. Extending to $(2+1)$D, the projected entangled pair state (PEPS) [29] provides a compelling theoretical framework of LGTs [13,17,27,30–33]. Nevertheless, PEPS-based simulations face substantial challenges stemming from both the intrinsic complexity of higher dimensionality and the rigorous requirements of gauge constraints. Recent explorations using gauge-invariant Gaussian PEPS [34–37] and non-gauge-constrained PEPS [38] have made first attempts for ground-state simulations of pure $\mathbb{Z}_2$ and $\mathbb{Z}_3$ LGTs. Nonetheless, advancing versatile and high-precision PEPS methodologies capable of tackling generic LGTs remains a crucial objective for both ground-state and dynamical studies, which is of great interest in light of current efforts to achieve quantum advantages for $(2+1)$D gauge theories on quantum computers [39,40] and ongoing needs to understand exotic quantum matter.

In this Letter, adopting the Hamiltonian formulation, we develop a PEPS-based computational framework to achieve accurate simulations of a wide range of $(2+1)$D Abelian LGTs. A key element is the identification of a gauge canonical form (GCF) for gauge-invariant (GI) TNS, with which we can already significantly simplify MPS-based methods in $(1+1)$D. In $(2+1)$D, the GCF enables a particularly efficient treatment of GI-PEPS via variational Monte Carlo (VMC), facilitating precise ground-state and dynamical calculations. Our method is extensively validated with ground-state simulations of $\mathbb{Z}_2$, $\mathbb{Z}_3$, and $\mathbb{Z}_4$ pure gauge theory, odd-$\mathbb{Z}_2$ gauge theory, and $\mathbb{Z}_2$ gauge theory coupled to hard-core bosons, on square lattices up to 32×32, and dynamical simulation of vison propagation in a deconfined $\mathbb{Z}_2$ gauge field. These results establish PEPS as a powerful pathway for accurate TNS simulations of $(2+1)$D Abelian LGTs, providing a new tool for

*These authors contributed equally to this work.
†Contact author: yantaow@iphy.ac.cn
‡Contact author: wyliu@zju.edu.cn

nonperturbatively studying LGTs and benchmarking quantum simulations.

Hamiltonian—We briefly review the LGT Hamiltonians [19,41]. A $(d+1)$D LGT is defined on a d-dimensional cubic lattice, with gauge fields on the links and matter fields on the vertices. For an Abelian gauge group $\mathbb{Z}_N$ [or U(1)], the link Hilbert space is spanned by the eigenstates $|n\rangle$ of an electric field operator E such that $E|n\rangle = n|n\rangle$, $n \in \mathbb{Z}_N$ (or $\mathbb{Z}$). Its raising operator $U \equiv e^{i\phi}$ is the exponential of its canonical conjugate operator ϕ: $[\phi, E] = i$ and $U|n\rangle = |n+1 \bmod N\rangle$. The matter Hilbert space hosts a boson or a fermion on the vertex $\mathbf{x}$ with annihilation operator $c_{\mathbf{x}}$. The gauge invariance, at every $\mathbf{x}$, is enforced as

$$c_{\mathbf{x}}^{\dagger} c_{\mathbf{x}} + \sum_{\alpha=1}^{d} (E_{(\mathbf{x}-\mathbf{e}_\alpha,\alpha)} - E_{(\mathbf{x},\alpha)}) = Q_{\mathbf{x}} \mod N, \quad (1)$$

where $(\mathbf{x}, \alpha)$ is a link between $\mathbf{x}$ and $\mathbf{x} + \mathbf{e}_\alpha$, with $\mathbf{e}_\alpha$ being the unit vector along the αth axis. $Q_{\mathbf{x}}$ is a preset integer, fixing the gauge sector. The LGT Hamiltonian is

$$H = H_M + H_B + H_E, \quad (2)$$

$$H_M = \sum_{\mathbf{x}} m_{\mathbf{x}} c_{\mathbf{x}}^{\dagger} c_{\mathbf{x}} + \sum_{\mathbf{x},\alpha} (J c_{\mathbf{x}}^{\dagger} U_{(\mathbf{x},\alpha)} c_{\mathbf{x}+\mathbf{e}_\alpha} + \text{H.c.}), \quad (3)$$

$$H_B = -h \sum_{\mathbf{x}} U_{\mathbf{x},1} U_{\mathbf{x}+\mathbf{e}_1,2} U_{\mathbf{x}+\mathbf{e}_2,1}^{\dagger} U_{\mathbf{x},2}^{\dagger} + \text{H.c.}, \quad (4)$$

$$H_E = g \sum_{\mathbf{x},\alpha} 2 - 2\cos(2\pi E_{(\mathbf{x},\alpha)}/N) \quad \text{or} \quad g \sum_{\mathbf{x},\alpha} E_{(\mathbf{x},\alpha)}^2, \quad (5)$$

where $m_{\mathbf{x}}$ is the chemical potential (or the bare particle mass). H_B and H_E are, respectively, the magnetic and electric energy terms. H_B is present only for $d \geq 2$, and the two instances of H_E are for either the $\mathbb{Z}_N$ or U(1) gauge group.

Gauge-invariant TNS—Gauge-invariant tensor-network states naturally describe the physical Hilbert space of LGTs [12–15,17,27,30,31]. To construct a GI-TNS wave function, one works in the basis of particle occupation number and electric fields. As in Fig. 1, the network has three-leg B tensors for gauge fields and $(2d+1)$-leg A tensors for matter fields. Gauge invariance of the wave function is enforced by imposing sparsity constraints on A and B. Specifically, we assign charges $q(j)$ in $\mathbb{Z}_N$ (or $\mathbb{Z}$) to tensor indices j on each virtual leg; then, in two spatial dimensions, tensor blocks of A and B satisfy [14]

$$A^{p}_{lrdu} = \mathcal{A}^{p}_{lrdu} \delta_{p+q(l)+q(d)-q(r)-q(u),Q_{\mathbf{x}}}, \quad (6)$$

$$B^{n}_{lr} = \mathcal{B}^{n}_{lr} \delta_{n,q(l)} \delta_{n,q(r)}. \quad (7)$$

The bond dimension of the TNS is then $D = \sum_k D_k$, where D_k is the degeneracy of the charge sector k, i.e., the number of tensor indices j with $q(j) = k$. Although this GI ansatz has been known for a decade, and its MPS algorithms has been established in $(1+1)$D [14], the algorithmic feasibility of GI-PEPS including optimization for ground-states and computation of physical quantities has remained a major roadblock, preventing the power of PEPS from manifesting for $(2+1)$D LGTs. Below, we show how to overcome these challenges.

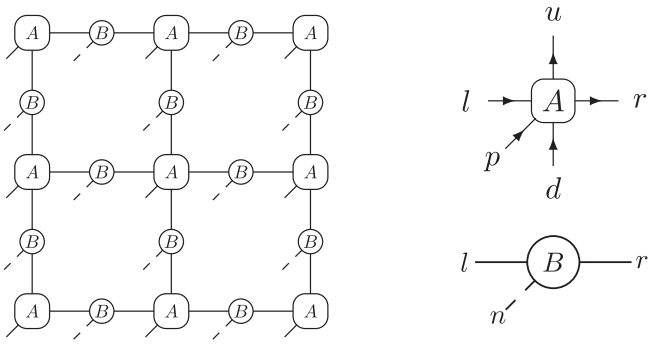

FIG. 1. Left is a diagram of a gauge-invariant PEPS for LGTs. Right are the matter tensor A and gauge tensor B. Here, d is the down leg of A and not the spatial dimension.

Gauge canonical form—A key ingredient for our approach is the GCF, which we now identify. On the link connecting an A tensor and a B tensor, one can define the following block-diagonal matrix:

$$X = \bigoplus_{k \in \mathbb{Z}_N (\text{or } \mathbb{Z})} \mathcal{B}^{[k]}, \quad (8)$$

where $\mathcal{B}^{[k]}$ is a $D_k \times D_k$ matrix obtained from choosing $n = k$ in B^n_{lr} and restricting to the l and r indices with charges equal to k. Using gauge transformations $A \to AX$ and $B \to X^{-1}B$, the gauge tensor B simplifies as

$$B^{n}_{lr} = \delta_{lr} \delta_{n,q(l)} \delta_{n,q(r)}, \quad (9)$$

and A keeps the same form as Eq. (6). We refer to this new form as the GCF, in which the B tensors no longer contain variational parameters and one needs only to optimize the A tensors. Below, we show how GCF enables efficient computations of GI-MPS (see End Matter) and GI-PEPS.

VMC—In 2D, GI-PEPS simulations are challenging due to their intrinsic complexity, gauge-invariance constraints, and the four-body plaquette terms in the Hamiltonian [Eq. (4)] [38]. We find that combining VMC and GCF overcomes these challenges effectively. In VMC, the expectation value of an observable is calculated as $\langle O \rangle = \sum_{\mathbf{s}} (|\langle \mathbf{s}|\Psi\rangle|^2/\langle\Psi|\Psi\rangle)(\langle \mathbf{s}|O|\Psi\rangle/\langle \mathbf{s}|\Psi\rangle)$, where $|\mathbf{s}\rangle$ labels a configuration of gauge and matter fields. This sum is estimated via sampling $|\mathbf{s}\rangle$ from the probability distribution $(|\langle \mathbf{s}|\Psi\rangle|^2/\langle\Psi|\Psi\rangle)$, where the basic component is evaluating single-layer networks $\langle \mathbf{s}|\Psi\rangle$ [42–46]. We

sample only physical configurations, as unphysical ones' amplitudes are exactly zero in GI-PEPS.

The sampling and GCF critically simplifies computations: Each configuration $|\mathbf{s}\rangle$ uniquely selects a single charge sector of matter tensors A with gauge tensors B absent. Thus, tensors in the resulting network $\langle \mathbf{s}|\Psi\rangle$ have only bond dimension D_k, significantly reduced from the total bond dimension $D = \sum_{k=1}^{N} D_k$ for $\mathbb{Z}_N$ gauge group. This allows efficient computations using advanced PEPS-VMC techniques [45–48] that have been used to study frustrated spin systems [49–54]. See Supplemental Material [55] for more discussions.

We use gradient-based stochastic reconfiguration [48,56,71,72] for both ground-state and real-time dynamics [57–59] of GI-PEPS for systems on the open square lattice. The computational cost scales as $O(D_k^5\chi^2 + D_k^4\chi^2 + D_k^3\chi^3)$, dominated by plaquette term evaluations and variational boundary MPS compression. χ is the cutoff bond dimension of the boundary MPS for contracting $\langle \mathbf{s}|\Psi\rangle$, with $\chi = 3D_k$ being good enough. Then, the energy measurement scales as $O(MN_{\text{site}}D_k^7)$, where N_{site} is the size and M is the number of Monte Carlo sweeps [55] typically on the order of 10^4 with statistical uncertainty about 10^{-5}.

Pure $\mathbb{Z}_N$ gauge theory—We first consider pure $\mathbb{Z}_2 - \mathbb{Z}_4$ gauge theories (no matter field, $Q_{\mathbf{x}} \equiv 0$). We use $D_k = 2$ which we find is good enough for convergence on relevant sizes (see Supplemental Material [55]). Fixing $h = 1$, we scan g to compute ground-state properties. For the well-understood $\mathbb{Z}_2$ pure gauge theory, the ground-state energies computed with GI-PEPS on the 16×16 lattice agree excellently with those of quantum Monte Carlo (QMC), showing high accuracy up to 10^{-5}. See more results in Supplemental Material [55].

For the $\mathbb{Z}_3$ case, we compute ground-state properties for sizes from 8×8 to 24×24. The first derivative of energy, $(\partial\langle H\rangle/\partial g) = (1/g)\langle H_E\rangle$ [Fig. 2(a)], and its finite-difference second derivative $(\partial^2\langle H\rangle/\partial g^2)$ [Fig. 2(b)] reveal clear signatures of a first-order transition, consistent with early studies [73]. The transition point from small sizes shows a minor shift. The convergence between 20×20 and 24×24 yields a thermodynamic-limit critical point at $g_c = 0.375(3)$. This agrees well with a recently found $g_c = 0.37(1)$ using neural quantum states on torus up to size 10×10 [60]. This is to be compared with the non-gauge-constrained iPEPS result $g_c = 0.448(3)$ [38], whose ground-state energies obtained near the critical region are higher than our results extrapolated to infinite size (see Supplemental Material [55]). The quantitative difference may arise from the reliance of iPEPS on simple update optimization rather than the fully variational optimization employed here, demonstrating the challenge of such calculations.

For the $\mathbb{Z}_4$ case, unexplored previously by TNS, we extend our analysis to 20×20 sites. As shown in Figs. 2(c) and 2(d), the energy derivatives suggest a phase transition

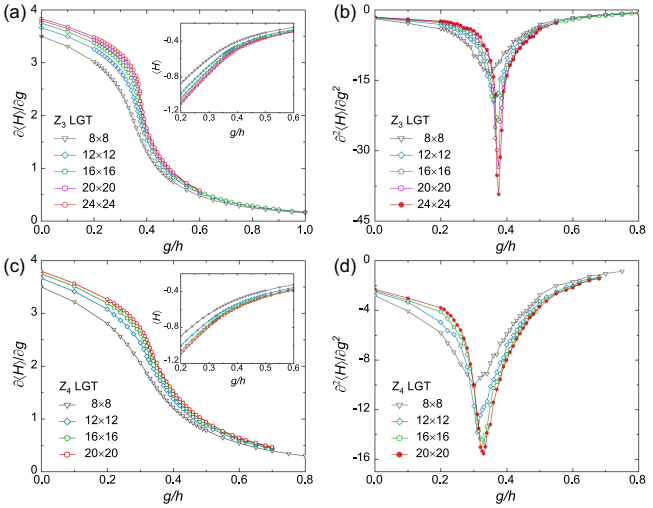

FIG. 2. Results of $\mathbb{Z}_3$ (a),(b) and $\mathbb{Z}_4$ (c),(d) LGTs at various g, including ground-state energy $\langle H\rangle$ [insets in (a) and (c)] and the first-order and second-order energy derivative.

at $g_c = 0.330(5)$, by comparing results from size 16×16 and 20×20. This constitutes the first PEPS study of $\mathbb{Z}_4$ LGT, offering a benchmark for higher-order gauge groups. Very interestingly, this g_c overlaps with that of the $\mathbb{Z}_2$ theory, 0.3285. In fact, for the 3D classical gauge theories, the $\mathbb{Z}_4$ theory is proven to be equivalent to the $\mathbb{Z}_2 \times \mathbb{Z}_2$ theory [74]. While no proof is available in the quantum case, we *conjecture* the equivalence here.

Odd-$\mathbb{Z}_2$ theory—Another representative example is the odd-$\mathbb{Z}_2$ gauge theory, i.e., with $Q_{\mathbf{x}} \equiv 1$ for all $\mathbf{x}$, relevant for understanding spin liquids and dimer models [75–78]. According to theoretical predictions [76–78], by varying g it experiences a continuous transition between a deconfined phase and a confined phase that breaks translation symmetry. Its dual model—the fully frustrated transverse field Ising model [77]—has been studied by QMC [79]. With GI-PEPS, we are able to directly obtain its ground-state *wave function*. Figures 3(a) and 3(b) show the plaquette operator $P_{\mathbf{x}} = U_{\mathbf{x},1}U_{\mathbf{x}+\mathbf{e}_1,2}U^{\dagger}_{\mathbf{x}+\mathbf{e}_2,1}U^{\dagger}_{\mathbf{x},2} + \text{H.c.}$ on a 32×32 lattice, revealing a uniform and a symmetry-broken phase at $g = 0.4$ and 0.8, respectively.

To precisely locate the transition point, we compute the valence-bond solid (VBS) order parameter [51]

$$D_{x/y} = \frac{1}{L(L-1)} \sum_{\mathbf{x}} (-1)^{x_\alpha} \bar{E}^{\alpha}_{\mathbf{x}}, \tag{10}$$

where $\alpha = 1, 2$ for D_x, D_y. $\bar{E}^{\alpha}_{\mathbf{x}} = 2 - 2\cos(\pi E_{(\mathbf{x},\alpha)})$ is the electric field strength on the link $(\mathbf{x}, \alpha)$ [see Eq. (5)], and $\mathbf{x} = (x_1, x_2)$ is the vertex position. Note the identical $\langle D_x\rangle^2$ and $\langle D_y\rangle^2$ in Fig. 3(c), which reflects the C_4 rotation symmetry. Through quadratic finite-size extrapolation, we obtain VBS order parameters in the thermodynamic limit [red curve in Fig. 3(c)], locating the phase transition point

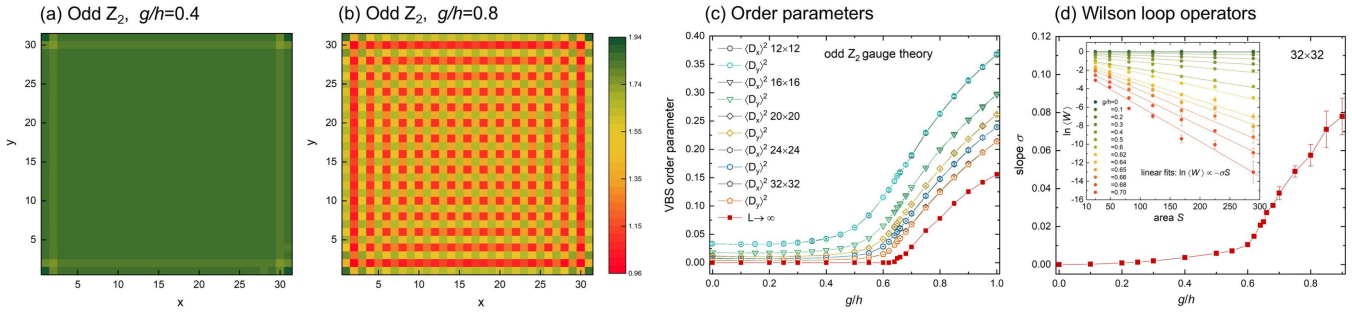

FIG. 3. Results of odd-$\mathbb{Z}_2$ LGT. (a) and (b) present the plaquette value $\langle P_{\mathbf{x}}\rangle$ at each site $\mathbf{x}$ on 32×32 at $g/h = 0.4$ and 0.8. (c) Shows the VBS order parameters $\langle D_x\rangle^2$ (black) and $\langle D_y\rangle^2$ (colorful), and red symbols are the values in thermodynamic limit extrapolated using quadratic fits of $\langle D_x\rangle^2$. The inset in (d) is the linear-linear plot of $\ln\langle W\rangle$ versus area S (different central regions on 32×32) to extract σ following $\langle W\rangle \propto e^{-\sigma S}$; the main panel shows the g dependence of the slope σ.

at $g_c = 0.64(1)$, in good agreement with the QMC results $g_c \simeq 0.634$ from the dual model [79].

The Wilson loop operator $\langle W\rangle$ on the 32×32 lattice is shown in Fig. 3(d). The slope σ, extracted from $\langle W\rangle \propto e^{-\sigma S}$, remains small for $g \lesssim 0.6$ but increases sharply afterward, signaling a perimeter-law to area-law transition consistent with $g_c = 0.64(1)$. These nonlocal operator calculations complements those of local operators $D_{x/y}$ in detecting translation symmetry breaking, providing insight into the underlying physics from the perspective of deconfinement.

$\mathbb{Z}_2$ gauge theory coupled to hard-core bosons—We demonstrate that we can directly deal with matter fields. Here, we consider $\mathbb{Z}_2$ gauge fields coupled to hard-core bosons. Its $(1+1)$D version has been studied, known as the $\mathbb{Z}_2$ Bose-Hubbard model [80], while the $(2+1)$D case remains uncharted. For benchmarking with exact diagonalization (ED) calculation, we first consider a 3×3 square lattice with two bosons. The definite boson number is realized by sampling in the corresponding particle number subspace. Taking $(h, g, J) = (1, 0.33, 0.5)$, the optimized $D = 6$ PEPS gives the energy per site $-0.470\,713\,502(3)$ using $M = 10^5$ samples, matching the ED energy $-0.470\,713\,506\,1$ excellently.

We then scale up to 16×16 sites at half filling of bosons. Figure 4(a) presents the energies from PEPS with bond dimensions D up to 14 for different sizes at $(h, g, J) = (1, 0.33, 0.5)$. Unlike the pure $\mathbb{Z}_2$ LGT, where $D = 4$ is sufficient, the matter-coupled case requires $D = 12$. These results reflect the increased entanglement of this model and our ability to handle large bond dimensions. We also compare the thermodynamic-limit energy evaluated using different central bulk energies for extrapolations [46,51]. Shown in Fig. 4(b), given a central bulk region of $L_b \times L_b$ [55], for example, $L_b = L - 2$, the extrapolated energy for the thermodynamic limit is $-1.3322(4)$, in good agreement with those from other choices of $L_b = L$ and $L_b = L - 4$ that are $-1.3337(4)$ and $-1.3322(2)$, respectively. This consistency corroborates our results [46,51].

One also expects that, in the presence of dynamical matter fields, the Wilson loop operator exhibits a perimeter law even in the confinement regime of the pure $\mathbb{Z}_2$ LGT, due to screening by the matter field [81]. This is indeed what we observe. We present the energy and Wilson loop operator of 16×16 lattice in Figs. 4(c) and 4(d). For pure $\mathbb{Z}_2$ LGT, as shown previously, $g = 0.2$, 0.33, and 0.4 correspond to the deconfined, near-critical, and confined regimes, respectively. From Fig. 4(d), we see after adding matter fields, at $g = 0.33$ and 0.4, that Wilson loop operators for different J show perimeter-law behavior.

Real-time dynamics in $(2+1)$D LGTs—A key advantage of the Hamiltonian formulation is its suitability for

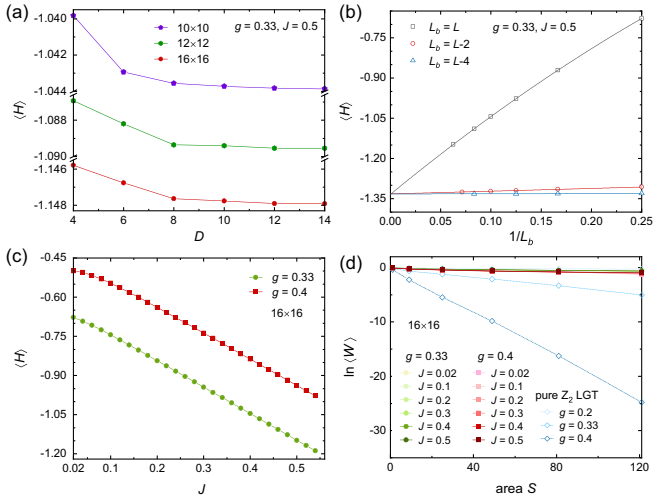

FIG. 4. Results of $\mathbb{Z}_2$ gauge field coupled to hard-core bosons at half filling ($h = 1$). (a) Convergence of energy with respect to bond dimensions. (b) Finite-size scaling of the energy using central bulk $L_b \times L_b$ energy of an $L\times L$ lattice. Quadratic fits are used for extrapolations. (c) J dependence of energy at $g = 0.33$ and 0.4 on 16×16 lattice. (d) Wilson loop operators on 16×16 lattice at different J for a given $g = 0.33$ (green) and $g = 0.4$ (red), compared to the pure $\mathbb{Z}_2$ LGT (blue). The green and red lines are, respectively, largely overlapped, both very close to the pure $\mathbb{Z}_2$ LGT at $g = 0.2$ (lightest blue).

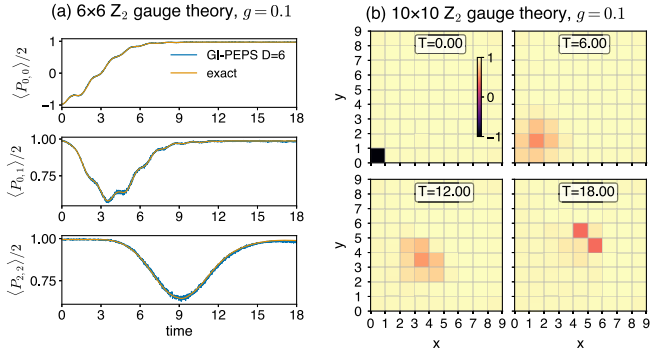

FIG. 5. Vison dynamics. The initial state is prepared by acting the Pauli matrix σ^z in the electric basis $\{|0\rangle, |1\rangle\}$ on the gauge field living on the bottom-left vertical link over the corresponding ground-state, in order to create a vison excitation. (a) Real-time dynamics of a vison (the value of $\langle P_x\rangle/2$) in a 6×6 lattice ($D = 6$), compared with exact diagonalizations. (b) Larger-scale simulation on 10×10 lattice showing vison propagation ($D = 6$ and $D = 8$ give the same result [55]).

studying real-time dynamics. Here, we directly demonstrate this capability by simulating the real-time evolution of a $\mathbb{Z}_2$ LGT using GI-PEPS. We use the scheme of time-dependent VMC (tVMC) [57,58], which recently has been applied to neural quantum states [61,82–87], and we adapt these techniques within our GI-PEPS framework. Notably, this Letter presents the first application of tVMC to PEPS, an advancement with potential implications far beyond gauge theory.

As a concrete example, we investigate the dynamics of a vison—an excitation of the deconfined $\mathbb{Z}_2$ gauge field corresponding to a violation of the plaquette operator $P_{\mathbf{x}} = U_{\mathbf{x},1}U_{\mathbf{x}+\mathbf{e}_1,2}U^\dagger_{\mathbf{x}+\mathbf{e}_2,1}U^\dagger_{\mathbf{x},2} + \text{H.c.}$ [76]. We initialize a vison at the bottom left of the lattice over the deconfined ground-state ($g = 0.1$) and evolve it under the same parameter, with a time step $\Delta t = 0.005$. On a 6×6 lattice, GI-PEPS reproduces the exact diagonalization results with high accuracy, as seen in the expectation values $\langle P_x\rangle/2$ at selected plaquettes [Fig. 5(a)]. On a 10×10 lattice, a system far beyond the reach of exact methods (Hilbert space dimension 2^{81}), the vison propagates cleanly toward the top right [Figs. 5(b)–5(d)], in a simulation time up to $T = 18$ (7200 evolution steps using second-order expansions [55]), while maintaining energy conservation within 0.2% [55]. This showcases the power of our approach in capturing long-time, large-scale quantum dynamics. See Supplemental Material [55] for a movie of the vison propagation and the details of the tVMC.

Conclusion and discussion—We have developed a powerful gauge-invariant tensor-network computational framework for $(2+1)$D Abelian LGTs, overcoming long-standing challenges in algorithmic feasibility of GI-PEPS. Central to our approach is the gauge canonical form, which fixes gauge tensors to parameter-free forms—thereby reducing variational parameters exclusively to matter tensors, as well as its further combination with VMC. We validate the framework across diverse models, achieving accurate large-scale simulations up to 32×32 sites for ground-states and 10×10 for dynamics. These advances establish gauge-invariant PEPS as a state-of-the-art tool for both ground-state and real-time dynamics simulations of Abelian LGTs. This framework opens up a new avenue for nonperturbative studies, and the GCF will be also potentially inspiring for non-Abelian cases. We believe this Letter will have a foundational impact on Hamiltonian-based approaches to LGTs. Generalization to fermionic matter is reserved for future work.

The potential of GI-PEPS and GCF remains to be seen for double-layer TNS methods [88]. Another possibility recently proposed is to modify the GI-PEPS ansatz as a symmetric PEPS by embedding the gauge group G into an enlarged globally symmetric theory with group $G\times G$ [89].

Acknowledgments—Y. W. thanks discussion with Akira Matsumoto, Etsuko Itou, Masazumi Honda, and Tetsuo Hatsuda during the early stage of the work. W.-Y. L. is especially grateful to Garnet K. Chan for encouragement. Y. W. is currently supported by a start-up grant from IOP-CAS. W.-Y. L. is supported by a start-up grant from Zhejiang University. Y. W. thanks Tao Xiang and Lei Wang for allowing him to use their computing resources. Part of the code is tested using the TenPy code base [90,91].

Data availability—The data that support the findings of this article are openly available [92]; embargo periods may apply.

[1] K. G. Wilson, Confinement of quarks, Phys. Rev. D **10**, 2445 (1974).
[2] J. B. Kogut, An introduction to lattice gauge theory and spin systems, Rev. Mod. Phys. **51**, 659 (1979).
[3] K. Fukushima and T. Hatsuda, The phase diagram of dense QCD, Rep. Prog. Phys. **74**, 014001 (2010).
[4] X.-G. Wen, *Quantum Field Theory of Many Body Systems: From the Origin of Sound to An Origin of Light and Electrons* (Oxford University Press, New York, 2004).
[5] A. Kitaev, Anyons in an exactly solved model and beyond, Ann. Phys. (Amsterdam) **321**, 2 (2006).
[6] M. Troyer and U.-J. Wiese, Computational complexity and fundamental limitations to fermionic quantum Monte Carlo simulations, Phys. Rev. Lett. **94**, 170201 (2005).
[7] C. Gross and I. Bloch, Quantum simulations with ultracold atoms in optical lattices, Science **357**, 995 (2017).
[8] C. D. Bruzewicz, J. Chiaverini, R. McConnell, and J. M. Sage, Trapped-ion quantum computing: Progress and challenges, Appl. Phys. Rev. **6**, 021314 (2019).
[9] P. Krantz, M. Kjaergaard, F. Yan, T. P. Orlando, S. Gustavsson, and W. D. Oliver, A quantum engineer's guide

to superconducting qubits, Appl. Phys. Rev. **6**, 021318 (2019).
[10] B. Yang, H. Sun, R. Ott, H.-Y. Wang, T. V. Zache, J. C. Halimeh, Z.-S. Yuan, P. Hauke, and J.-W. Pan, Observation of gauge invariance in a 71-site Bose-Hubbard quantum simulator, Nature (London) **587**, 392 (2020).
[11] M. C. Banuls *et al.*, Simulating lattice gauge theories within quantum technologies, Eur. Phys. J. D **74**, 165 (2020).
[12] L. Tagliacozzo and G. Vidal, Entanglement renormalization and gauge symmetry, Phys. Rev. B **83**, 115127 (2011).
[13] L. Tagliacozzo, A. Celi, and M. Lewenstein, Tensor networks for lattice gauge theories with continuous groups, Phys. Rev. X **4**, 041024 (2014).
[14] B. Buyens, J. Haegeman, K. Van Acoleyen, H. Verschelde, and F. Verstraete, Matrix product states for gauge field theories, Phys. Rev. Lett. **113**, 091601 (2014).
[15] P. Silvi, E. Rico, T. Calarco, and S. Montangero, Lattice gauge tensor networks, New J. Phys. **16**, 103015 (2014).
[16] H. Zou, Y. Liu, C.-Y. Lai, J. Unmuth-Yockey, L.-P. Yang, A. Bazavov, Z. Y. Xie, T. Xiang, S. Chandrasekharan, S.-W. Tsai, and Y. Meurice, Progress towards quantum simulating the classical O(2) model, Phys. Rev. A **90**, 063603 (2014).
[17] J. Haegeman, K. Van Acoleyen, N. Schuch, J. I. Cirac, and F. Verstraete, Gauging quantum states: From global to local symmetries in many-body systems, Phys. Rev. X **5**, 011024 (2015).
[18] Y. Kuramashi and Y. Yoshimura, Three-dimensional finite temperature $\mathbb{Z}_2$ gauge theory with tensor network scheme, J. High Energy Phys. 08 (2019) 023.
[19] P. Emonts and E. Zohar, Gauss law, minimal coupling and fermionic PEPS for lattice gauge theories, SciPost Phys. Lect. Notes 12 (2020).
[20] T. Felser, P. Silvi, M. Collura, and S. Montangero, Two-dimensional quantum-link lattice quantum electrodynamics at finite density, Phys. Rev. X **10**, 041040 (2020).
[21] G. Magnifico, T. Felser, P. Silvi, and S. Montangero, Lattice quantum electrodynamics in $(3+1)$-dimensions at finite density with tensor networks, Nat. Commun. **12**, 3600 (2021).
[22] Y. Meurice, R. Sakai, and J. Unmuth-Yockey, Tensor lattice field theory for renormalization and quantum computing, Rev. Mod. Phys. **94**, 025005 (2022).
[23] G. Cataldi, G. Magnifico, P. Silvi, and S. Montangero, Simulating $(2+1)$D SU(2) Yang-Mills lattice gauge theory at finite density with tensor networks, Phys. Rev. Res. **6**, 033057 (2024).
[24] T. Byrnes, P. Sriganesh, R. Bursill, and C. Hamer, Density matrix renormalisation group approach to the massive Schwinger model, Nucl. Phys. **B109**, 202 (2002).
[25] T. M. R. Byrnes, P. Sriganesh, R. J. Bursill, and C. J. Hamer, Density matrix renormalization group approach to the massive Schwinger model, Phys. Rev. D **66**, 013002 (2002).
[26] M. C. Bañuls, K. Cichy, J. I. Cirac, and K. Jansen, The mass spectrum of the Schwinger model with matrix product states, J. High Energy Phys. 11 (2013) 158.
[27] E. Rico, T. Pichler, M. Dalmonte, P. Zoller, and S. Montangero, Tensor networks for lattice gauge theories and atomic quantum simulation, Phys. Rev. Lett. **112**, 201601 (2014).
[28] M. Carmen Bañuls and K. Cichy, Review on novel methods for lattice gauge theories, Rep. Prog. Phys. **83**, 024401 (2020).
[29] F. Verstraete and J. I. Cirac, Renormalization algorithms for quantum-many body systems in two and higher dimensions, arXiv:cond-mat/0407066.
[30] E. Zohar, M. Burrello, T. B. Wahl, and J. I. Cirac, Fermionic projected entangled pair states and local U(1) gauge theories, Ann. Phys. (Amsterdam) **363**, 385 (2015).
[31] E. Zohar and M. Burrello, Building projected entangled pair states with a local gauge symmetry, New J. Phys. **18**, 043008 (2016).
[32] D. Blanik, J. Garre-Rubio, A. Molnár, and E. Zohar, Internal structure of gauge-invariant projected entangled pair states, J. Phys. A **58**, 065301 (2025).
[33] G. Roose and E. Zohar, Superposing and gauging fermionic gaussian projected entangled pair states to get exact lattice gauge theory groundstates, arXiv:2412.01737.
[34] E. Zohar and J. I. Cirac, Combining tensor networks with monte carlo methods for lattice gauge theories, Phys. Rev. D **97**, 034510 (2018).
[35] P. Emonts, A. Kelman, U. Borla, S. Moroz, S. Gazit, and E. Zohar, Finding the ground state of a lattice gauge theory with fermionic tensor networks: A $2+1d$ $\mathbb{Z}_2$ demonstration, Phys. Rev. D **107**, 014505 (2023).
[36] P. Emonts, M. C. Bañuls, I. Cirac, and E. Zohar, Variational Monte Carlo simulation with tensor networks of a pure Z_3 gauge theory in $2+1$ D, Phys. Rev. D **102**, 074501 (2020).
[37] A. Kelman, U. Borla, I. Gomelski, J. Elyovich, G. Roose, P. Emonts, and E. Zohar, Gauged gaussian projected entangled pair states: A high dimensional tensor network formulation for lattice gauge theories, Phys. Rev. D **110**, 054511 (2024).
[38] D. Robaina, M. C. Bañuls, and J. I. Cirac, Simulating $2+1$ D $\mathbb{Z}_3$ lattice gauge theory with an infinite projected entangled-pair state, Phys. Rev. Lett. **126**, 050401 (2021).
[39] T. Cochran, B. Jobst, E. Rosenbeg, Y. D. Lensky, G. Grawali *et al.*, Visualizing dynamics of charges and strings in $(2+1)$d lattice gauge theories, Nature (London) **642**, 315 (2025).
[40] A. Crippa, K. Jansen, and E. Rinaldi, Analysis of the confinement string in $(2+1)$-dimensional quantum electrodynamics with a trapped-ion quantum computer, arXiv:2411.05628.
[41] J. Kogut and L. Susskind, Hamiltonian formulation of Wilson's lattice gauge theories, Phys. Rev. D **11**, 395 (1975).
[42] A. W. Sandvik and G. Vidal, Variational quantum Monte Carlo simulations with tensor-network states, Phys. Rev. Lett. **99**, 220602 (2007).
[43] N. Schuch, M. M. Wolf, F. Verstraete, and J. I. Cirac, Simulation of quantum many-body systems with strings of operators and Monte Carlo tensor contractions, Phys. Rev. Lett. **100**, 040501 (2008).
[44] L. Wang, I. Pižorn, and F. Verstraete, Monte Carlo simulation with tensor network states, Phys. Rev. B **83**, 134421 (2011).
[45] W.-Y. Liu, S.-J. Dong, Y.-J. Han, G.-C. Guo, and L. He, Gradient optimization of finite projected entangled pair states, Phys. Rev. B **95**, 195154 (2017).

[46] W.-Y. Liu, Y.-Z. Huang, S.-S. Gong, and Z.-C. Gu, Accurate simulation for finite projected entangled pair states in two dimensions, Phys. Rev. B **103**, 235155 (2021).

[47] W.-Y. Liu, S.-J. Du, R. Peng, J. Gray, and Garnet Kin-Lic Chan, Tensor network computations that capture strict variationality, volume law behavior, and the efficient representation of neural network states, Phys. Rev. Lett. **133**, 260404 (2024).

[48] W.-Y. Liu, H. Zhai, R. Peng, Z.-C. Gu, and G. K.-L. Chan, Accurate simulation of the Hubbard model with finite fermionic projected entangled pair states, Phys. Rev. Lett. **134**, 256502 (2025).

[49] W.-Y. Liu, S. Dong, C. Wang, Y. Han, H. An, G.-C. Guo, and L. He, Gapless spin liquid ground state of the spin-$\frac{1}{2}$ $J_1 - J_2$ Heisenberg model on square lattices, Phys. Rev. B **98**, 241109(R) (2018).

[50] W.-Y. Liu, S.-S. Gong, Y.-B. Li, D. Poilblanc, W.-Q. Chen, and Z.-C. Gu, Gapless quantum spin liquid and global phase diagram of the spin-1/2 $J_1 - J_2$ square antiferromagnetic Heisenberg model, Sci. Bull. **67**, 1034 (2022).

[51] W.-Y. Liu, J. Hasik, S.-S. Gong, D. Poilblanc, W.-Q. Chen, and Z.-C. Gu, Emergence of gapless quantum spin liquid from deconfined quantum critical point, Phys. Rev. X **12**, 031039 (2022).

[52] W.-Y. Liu, S.-S. Gong, W.-Q. Chen, and Z.-C. Gu, Emergent symmetry in quantum phase transition: From deconfined quantum critical point to gapless quantum spin liquid, Sci. Bull. **69**, 190 (2024).

[53] W.-Y. Liu, D. Poilblanc, S.-S. Gong, W.-Q. Chen, and Z.-C. Gu, Tensor network study of the spin-$\frac{1}{2}$ square-lattice $J_1 - J_2 - J_3$ model: Incommensurate spiral order, mixed valence-bond solids, and multicritical points, Phys. Rev. B **109**, 235116 (2024).

[54] W.-Y. Liu, X.-T. Zhang, Z. Wang, S.-S. Gong, W.-Q. Chen, and Z.-C. Gu, Quantum criticality with emergent symmetry in the extended Shastry-Sutherland model, Phys. Rev. Lett. **133**, 026502 (2024).

[55] See Supplemental Material at http://link.aps.org/supplemental/10.1103/3m3j-ds18 for additional computational details and a movie of the vison propagation, which includes Refs. [34–38,42–54,56–70].

[56] S. Sorella, Green function Monte Carlo with stochastic reconfiguration, Phys. Rev. Lett. **80**, 4558 (1998).

[57] G. Carleo, F. Becca, M. Schiró, and M. Fabrizio, Localization and glassy dynamics of many-body quantum systems, Sci. Rep. **2**, 243 (2012).

[58] G. Carleo, F. Becca, L. Sanchez-Palencia, S. Sorella, and M. Fabrizio, Light-cone effect and supersonic correlations in one- and two-dimensional bosonic superfluids, Phys. Rev. A **89**, 031602(R) (2014).

[59] K. Ido, T. Ohgoe, and M. Imada, Time-dependent many-variable variational monte carlo method for nonequilibrium strongly correlated electron systems, Phys. Rev. B **92**, 245106 (2015).

[60] A. Apte, C. Córdova, T.-C. Huang, and A. Ashmore, Deep learning lattice gauge theories, Phys. Rev. B **110**, 165133 (2024).

[61] J. Nys, G. Pescia, A. Sinibaldi, and G. Carleo, Ab-initio variational wave functions for the time-dependent many-electron schrödinger equation, Nat. Commun. **15**, 9404 (2024).

[62] S.-J. Dong, C. Wang, Y. Han, G. C. Guo, and L. He, Gradient optimization of fermionic projected entangled pair states on directed lattices, Phys. Rev. B **99**, 195153 (2019).

[63] S.-J. Dong, C. Wang, Y.-J. Han, C. Yang, and L. He, Stable diagonal stripes in the $t - J$ model at $\bar{n}_h = 1/8$ doping from fPEPS calculations, npj Quantum Mater. **5**, 28 (2020).

[64] Y. Wu and Z. Dai, Algorithms for variational Monte Carlo calculations of fermion PEPS in the swap gates formulation, arXiv:2506.20106.

[65] F. Becca and S. Sorella, *Quantum Monte Carlo Approaches for Correlated Systems* (Cambridge University Press, Cambridge, England, 2017).

[66] F. Verstraete, V. Murg, and J. I. Cirac, Matrix product states, projected entangled pair states, and variational renormalization group methods for quantum spin systems, Adv. Phys. **57**, 143 (2008).

[67] G. Vidal, Classical simulation of infinite-size quantum lattice systems in one spatial dimension, Phys. Rev. Lett. **98**, 070201 (2007).

[68] J. Haegeman, J. I. Cirac, T. J. Osborne, I. Pižorn, H. Verschelde, and F. Verstraete, Time-dependent variational principle for quantum lattices, Phys. Rev. Lett. **107**, 070601 (2011).

[69] J. Haegeman, C. Lubich, I. Oseledets, B. Vandereycken, and F. Verstraete, Unifying time evolution and optimization with matrix product states, Phys. Rev. B **94**, 165116 (2016).

[70] F. Wu, Y. Deng, and N. Prokof'ev, Phase diagram of the toric code model in a parallel magnetic field, Phys. Rev. B **85**, 195104 (2012).

[71] S. Sorella, Generalized Lanczos algorithm for variational quantum Monte Carlo, Phys. Rev. B **64**, 024512 (2001).

[72] T. Vieijra, J. Haegeman, F. Verstraete, and L. Vanderstraeten, Direct sampling of projected entangled-pair states, Phys. Rev. B **104**, 235141 (2021).

[73] G. Bhanot and M. Creutz, Phase diagram of Z(N) and U(1) gauge theories in three dimensions, Phys. Rev. D **21**, 2892 (1980).

[74] H. Grosse, C. Lang, and H. Nicolai, Equivalence of the z_4 and the $z_2 \times z_2$ lattice gauge theories, Phys. Lett. B **98**, 69 (1981).

[75] R. A. Jalabert and S. Sachdev, Spontaneous alignment of frustrated bonds in an anisotropic, three-dimensional ising model, Phys. Rev. B **44**, 686 (1991).

[76] T. Senthil and M. P. A. Fisher, Z_2 gauge theory of electron fractionalization in strongly correlated systems, Phys. Rev. B **62**, 7850 (2000).

[77] R. Moessner, S. L. Sondhi, and E. Fradkin, Short-ranged resonating valence bond physics, quantum dimer models, and ising gauge theories, Phys. Rev. B **65**, 024504 (2001).

[78] S. Sachdev, Topological order, emergent gauge fields, and fermi surface reconstruction, Rep. Prog. Phys. **82**, 014001 (2018).

[79] S. Wenzel, T. Coletta, S. E. Korshunov, and F. Mila, Evidence for columnar order in the fully frustrated transverse field ising model on the square lattice, Phys. Rev. Lett. **109**, 187202 (2012).

[80] D. González-Cuadra, A. Dauphin, P. R. Grzybowski, P. Wójcik, M. Lewenstein, and A. Bermudez, Symmetry-breaking topological insulators in the $\mathbb{Z}_2$ Bose-Hubbard model, Phys. Rev. B **99**, 045139 (2019).
[81] E. Fradkin, *Fideld Theories of Condensed Matter Physics* (Cambridge University Press, Cambridge, England, 2013).
[82] G. Carleo, L. Cevolani, L. Sanchez-Palencia, and M. Holzmann, Unitary dynamics of strongly interacting Bose gases with the time-dependent variational monte carlo method in continuous space, Phys. Rev. X **7**, 031026 (2017).
[83] M. Schmitt and M. Heyl, Quantum many-body dynamics in two dimensions with artificial neural networks, Phys. Rev. Lett. **125**, 100503 (2020).
[84] I. L. Gutiérrez and C. B. Mendl, Real time evolution with neural-network quantum states, Quantum **6**, 627 (2022).
[85] M. Gartner, F. Mazzanti, and R. E. Zillich, Time-dependent variational Monte Carlo study of the dynamic response of bosons in an optical lattice, SciPost Phys. **13**, 025 (2022).
[86] A. Sinibaldi, C. Giuliani, G. Carleo, and F. Vicentini, Unbiasing time-dependent variational Monte Carlo by projected quantum evolution, Quantum **7**, 1131 (2023).
[87] M. Medvidović and D. Sels, Variational quantum dynamics of two-dimensional rotor models, PRX Quantum **4**, 040302 (2023).
[88] We thank Jutho Haegeman for sending us a recent unpublished master thesis from his group, where exact gradient descent using automatic differentiation was attempted for finding the ground-states of an infinite PEPS with structure similar to GCF. Although the numerical results are yet to converge with the bond dimension in the thesis, they do show the possibility of such calculations using more conventional methods based on double-layer TNS contraction.
[89] M. Canals, N. Chepiga, and L. Tagliacozzo, A tensor network formulation of lattice gauge theories based only on symmetric tensors, arXiv:2412.16961.
[90] J. Hauschild and F. Pollmann, Efficient numerical simulations with Tensor networks: Tensor Network Python (TenPy), SciPost Phys. Lect. Notes 5 (2018).
[91] J. Hauschild *et al.*, Tensor network Python (TenPy) version 1, SciPost Phys. Codebases 41 (2024).
[92] Y. Wu and W.-Y. Liu, github data repository, https://github.com/yantaow/open_data/tree/main/wu2025accurate (2025).
[93] G. Vidal, Efficient classical simulation of slightly entangled quantum computations, Phys. Rev. Lett. **91**, 147902 (2003).
[94] J. Schwinger, Gauge invariance and mass. II, Phys. Rev. **128**, 2425 (1962).
[95] Q.-Q. Shi, S.-H. Li, J.-H. Zhao, and H.-Q. Zhou, Graded projected entangled-pair state representations and an algorithm for translationally invariant strongly correlated electronic systems on infinite-size lattices in two spatial dimensions, arXiv:0907.5520.
[96] P. Corboz, R. Orús, B. Bauer, and G. Vidal, Simulation of strongly correlated fermions in two spatial dimensions with fermionic projected entangled-pair states, Phys. Rev. B **81**, 165104 (2010).
[97] Provided by Akira Matsumoto.

End Matter

GCF in $(1+1)$D—In End Matter, we demonstrate that the GCF enables an elegant algorithm of the time evolution block decimation (TEBD) [93] for LGT in $(1+1)$D. We take the Schwinger model as an example, which is a toy model of quantum electrodynamic in $(1+1)$D [94]. Its Hamiltonian is $H_M + H_E$ with U(1) gauge group and staggered fermions $Q_x = [1+(-1)^x]/2$ and $m_x = (-1)^x m$.

Because of the GCF, simulations do not explicitly require the gauge tensors. Instead, the time evolution of the Schwinger model is simulated via a U(1)-symmetric TEBD applied to the Hamiltonian with global symmetry:

$$H = \sum_x m_x c_x^\dagger c_x + \sum_x J c_x^\dagger c_{x+1} + \text{H.c.}, \qquad \text{(A1)}$$

with an MPS made only of A tensors. The would-be gauge canonical B tensors dictate that the virtual charges of A encode the physical electric fields. Instead of using Jordan-Wigner transformation, we directly use the fermionic MPS in the swap gate formalism [95,96].

Simulating Eq. (A1) is different from the LGT systems in three aspects: (1) The electric part $H_E = g\sum_x E_x^2$ is missing. (2) The hopping $c_x^\dagger c_{x+1}$ is different from the gauge-invariant hopping $c_x^\dagger U_x c_{x+1}$. (3) For systems with global symmetry, there is an arbitrariness in the symmetry charge of the MPS tensors A_x. Suppose one has tensor A_x and A_{x+1}, with symmetry charge Q_x and Q_{x+1}. Combining A_x and A_{x+1} gives a two-site tensor $\Lambda \equiv A_x A_{x+1}$, with symmetry charge $Q_x + Q_{x+1}$. The TEBD gate tensor U changes Λ to Λ' but does not change the symmetry charge of Λ. When one splits Λ' to A'_x and A'_{x+1} via singular value decomposition, one can assign any symmetry charge Q'_x to A'_x as long as A'_{x+1}'s symmetry charge is then assigned as $Q_x + Q_{x+1} - Q'_x$ and the virtual charge on the link between x and $x+1$ properly redefined. This arbitrariness is absent for LGTs, as the symmetry charge Q_x is predefined. To accommodate these differences, two additions are needed during the TEBD of Eq. (A1): (1) At each link, apply the time evolution gate $e^{-id\tau g E_x^2}$ [Eq. (5)] ($d\tau$ being the time step) on the virtual charges of A_x. (ii) Keep the symmetry charge of A_x as Q_x when splitting a two-site wave function $A_x A_{x+1}$. During the TEBD of Eq. (A1), the hopping term $c_x^\dagger c_{x+1}$ shifts the symmetry charge of A_x (A_{x+1}) by $+1$ (-1). One can exploit the gauge freedom of the symmetry charges in an MPS with global symmetry to redefine the postsplit tensors' symmetry charges—reverting A_x's to Q_x and A_{x+1}'s to Q_{x+1}—while incrementing the virtual charge

between x and $x+1$ by $+1$. This precisely implements the gauge-invariant $c_x^\dagger U_x c_{x+1}$, as summarized in Fact 1.

Fact 1—Let A'_x and A'_{x+1} be the result of $c_x^\dagger c_{x+1}$ acting on the two-site wave function $A_x A_{x+1}$:

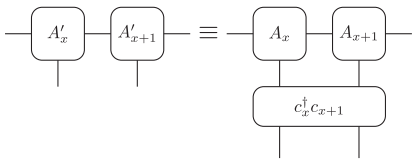

(B1)

Then,

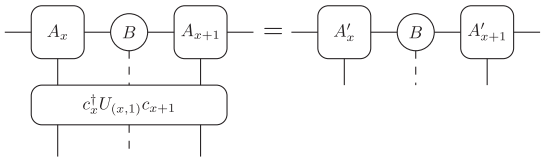

(B2)

where B is in GCF.

Another important piece of the TEBD algorithm is the MPS isometric canonical form (not to be confused with the gauge canonical form): The truncation of the two-site wave function must be performed at the canonical center. The isometric canonical form is also preserved by the GCF due to the following equation:

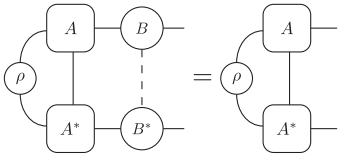

(B3)

provided that B is in GCF.

The approach described here significantly simplifies the algorithm of Ref. [14] without any approximation, which required manual gauge field truncation and blocking of A and B tensors. For example, if one cuts the gauge field at $|n|_{\max} = 3$, then a physical leg dimension of 14 is needed on each site in [14], while for us the physical dimension is always 2. In addition, our cutoff of the gauge field is based on entanglement via singular value decomposition, which seems much more natural for an MPS.

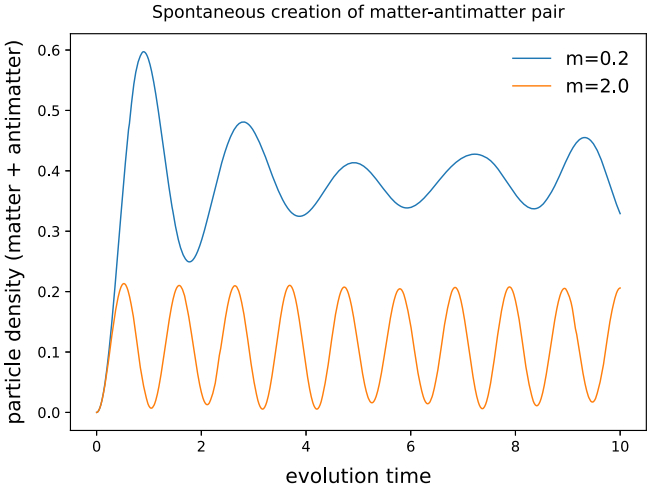

FIG. 6. Schwinger mechanism on a 40-site chain. $J = i$, $g = 1$. The time evolution is obtained using TEBD with a second-order Trotter decomposition with time step $dt = 0.01$.

To validate our method, we perform imaginary-time evolution ($d\tau = 0.01$) on a 16-site chain with $m = 0.2$, $J = -5i$, $g = 0.05$ and obtained ground-state energy $-36.339\,90$, which is in excellent agreement with exact diagonalization ($-36.339\,94$) [97]. Figure 6 further illustrates real-time evolution starting from the vacuum state: Particle-antiparticle pairs are spontaneously created, and smaller fermion masses m enhance particle-antiparticle pair production, directly manifesting the Schwinger mechanism [94].